Natural Resources Research, Vol. 32, No. 6, December 2023 (© 2023)
https://doi.org/10.1007/s11053-023-10263-8

Original Paper

Study on Impact Dynamic Behavior and Failure Characteristics of Coal based on True Triaxial Split–Hopkinson Pressure Bar Experiments

Rongxi Shen,[1,2] Zhoujie Gu,[1,2,3] Zhentang Liu,[1,2] Enlai Zhao,[1,2] Zesheng Zang,[1,2] Xin Zhou,[1,2] Xiaoliang Li,[1,2] Wei Liu,[1,2] and Xi Wang[1,2]

Received 21 March 2023; accepted 29 September 2023
Published online: 18 October 2023

Full understanding of dynamic mechanical characteristics of coal samples under true triaxial condition is of great significance for preventing and controlling deep coal and rock dynamic disasters. The results of this study showed that the transmission amplitude decreases with the increase in σ_1 and increases with the increase in the impact velocity. The peak stress and absorbed energy of coal decreased with the increase in σ_1 under true triaxial conditions. Under uniaxial and true triaxial conditions, the peak stress and absorbed energy of coal increased with the increase in impact velocity, and the stress change under true triaxial conditions was more sensitive to the action of dynamic load. Compared with uniaxial impact, the damage degree of coal sample under true triaxial condition was lower. The fractal dimension of broken blocks increased linearly with the increase in σ_1 and dynamic load, indicating that the degree of broken coal was intensified. This study effectively reveals the failure mechanism of coal under unequal static load and dynamic load.

KEY WORDS: True triaxial, SHPB, Stress evolution, Failure mechanism.

INTRODUCTION

As coal mining enters into the deep, coal rock is generally in a multidimensional stress state due to the coupling effect of high static stress and strong dynamic disturbance (He et al. 2015; Peng et al. 2015; Duan et al. 2021; Li et al. 2023a). Taking deep mining as an example (Zhang et al. 2014) (Fig. 1), deep coal and surrounding rock are subjected to high static stress such as self-weight stress and tectonic stress (Du et al. 2021; Wang et al. 2022a), accompanied by dynamic load such as explosive blasting and mechanical drilling. The stress state of coal at depth undergoes three-dimensional (3D), two-dimensional and one-dimensional (1D) conditions (Zhang et al. 2014; Liu et al. 2019; Liu et al. 2023; Wang et al. 2023; Zhou et al. 2023). Therefore, the study of mechanical behavior and deformation capacity of coal and rock under true triaxial prestress has more extensive application in engineering practice.

The SHPB (Split–Hopkinson pressure bar) device is used widely for dynamic testing of coal and rock materials (Grote et al. 2001; Zhang et al. 2014; Feng et al. 2022; Song et al. 2022; Li et al. 2023b, 2023c). Scholars have successively carried out several uniaxial studies (Liu et al. 2015; Zhao et al.

[1]Key Laboratory of Gas and Fire Control for Coal Mines, Ministry of Education, China University of Mining and Technology, Xuzhou 221116, Jiangsu, China.
[2]School of Safety Engineering, China University of Mining and Technology, Xuzhou 221116, Jiangsu, China.
[3]To whom correspondence should be addressed; e-mail: guzhoujie1996@126.com

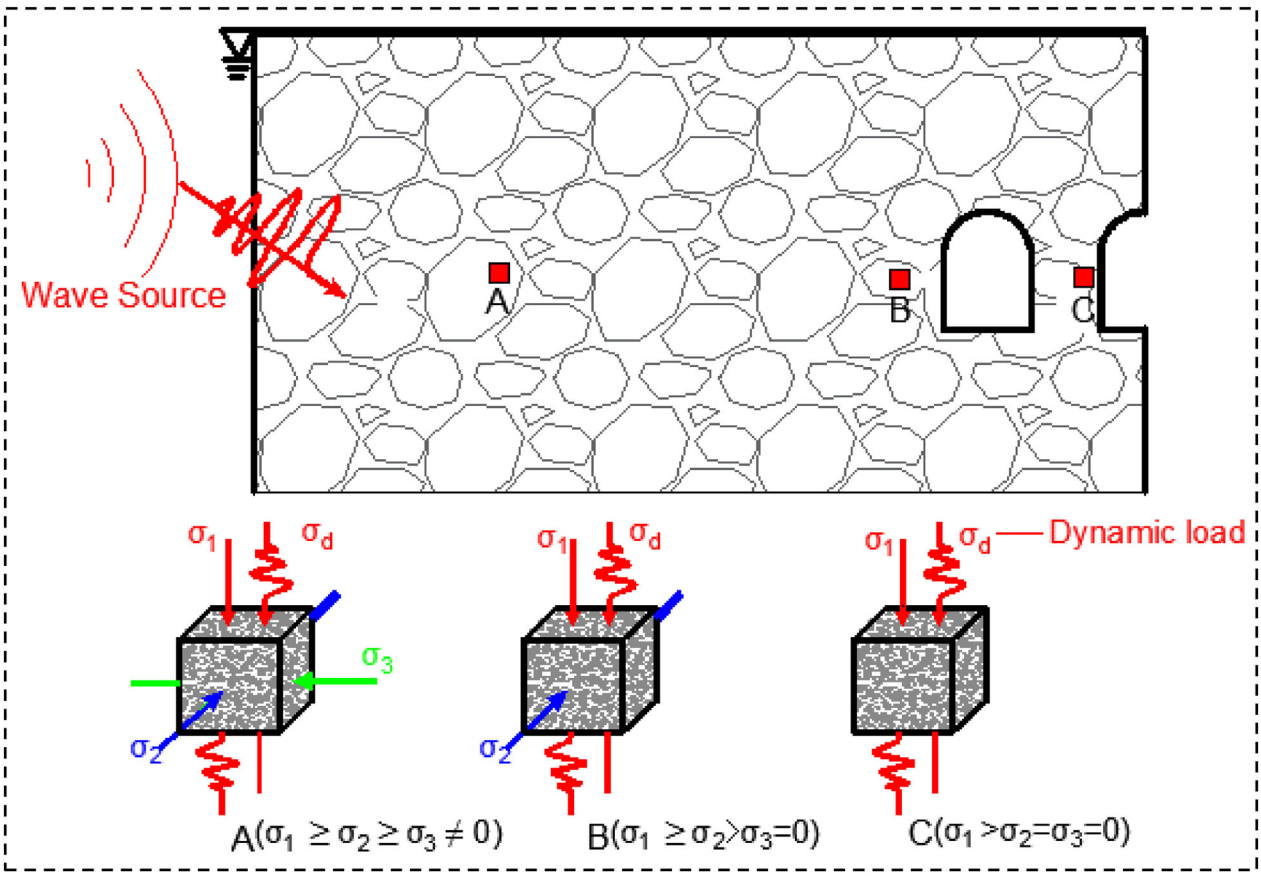

Figure 1. Stress evolution process of coal rock.

2017; Li et al. 2018, 2021a; Yu et al. 2019; Huang et al. 2021; Tan et al. 2023; Gu et al. 2023a) and conventional triaxial (Yin et al. 2012; Chen et al. 2018; Kong et al. 2020; Li et al. 2022; Zhu et al. 2022) studies on coal and rock materials. The mechanical properties, energy characteristics and failure forms of coal samples under uniaxial and conventional triaxial conditions have been analyzed experimentally. In recent years, scholars have developed a true triaxial SHPB impact test device (Liu et al. 2020a, 2020b; Xu et al. 2020; Xie et al. 2021; Luo et al. 2022; Gong et al. 2023) for specimens subjected to 3D unequal prestress. Liu et al. (2019, 2020a) and Wei et al. (2023) conducted true triaxial impact experiments on rock and concrete, and concluded that the mechanical strength of rock and concrete decreases with the increase in σ_1 (maximum principal stress) and gradually increases with the increase σ_2 and σ_3. The failure mode of rock under high prestress is shear fracture. Hu et al. (2020) analyzed that the mechanical strength of rock under true triaxial conditions decreases with the increase in σ_1 and increases with the increase in strain rate by numerical simulation. Through the combination of experiment and numerical simulation, You et al. (2022a) studied and found that the dynamic strength of rock samples under triaxial conditions gradually decreases with the increase in axial compression σ_1, while the total strength hardly changes. Liu et al. (2020b), Wang et al. (2021a, 2021b, 2021c, 2021d) and Chen et al. (2023) revealed that the mechanical strength of rock and concrete gradually increases with an increase in the impact load under true triaxial conditions. Compared with rock and concrete materials, studies on coal samples mainly focused on uniaxial and conventional triaxial impact. Kong et al. (2021) concluded that the dynamic strength of conventional triaxial coal samples decreases with the increase in axial pressure and increases with the increase in impact velocity. Wang et al. (2022a, 2022b) found

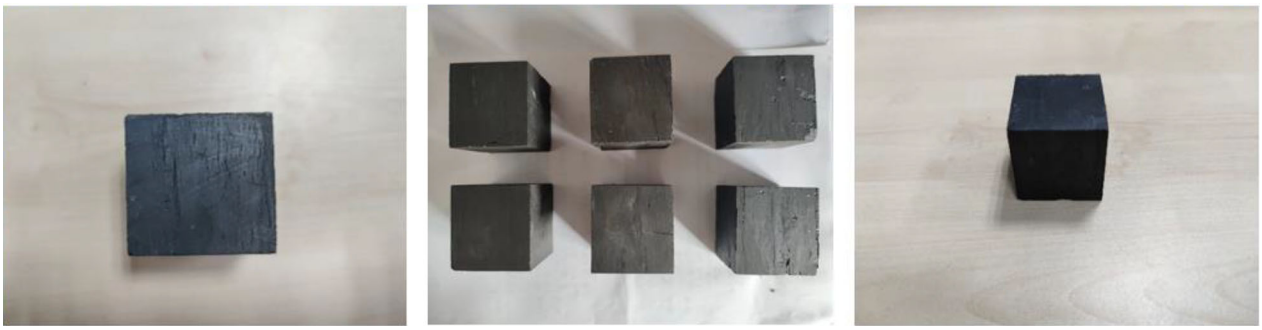

Figure 2. Coal samples.

that the dynamic strength of coal samples increases first and then decreases with the increase in axial pressure, and increases with the increase in impact velocity under uniaxial conditions. Ji et al. (2023) found that the damage of coal samples increases with the increase in prestress difference.

Uniaxial ($\sigma_1 \geq \sigma_2 = \sigma_3 = 0$) tests and conventional triaxial ($\sigma_1 \neq \sigma_2 = \sigma_3 > 0$) SHPB tests have been conducted on coal substantially, whereas true 3D ($\sigma_1 \neq \sigma_2 \neq \sigma_3$) dynamic tests on coal are rarely mentioned. It is necessary to fully understand the influence of axial dynamic–static load interaction on the mechanical behavior of coal samples under the three-way unequal binding force. In this paper, experiments were performed under different static prestress and impact velocities. The stress evolution, energy storage mechanism and failure mode of coal mass were analyzed. The mechanism of coal fracture was also studied in different three-way prestress and dynamic load.

EXPERIMENT

Experimental Sample and Apparatus

The coal samples used in the experiment were collected from Inner Mongolia, China. These samples boast good integrity and homogeneity. To carry out the impact experiment, all samples were processed into a cube shape with a side length of 47 mm (Fig. 2). To ensure homogeneity, all samples were taken from the same coal block and tested for weighing before the test. The average density of coal samples was measured to be about 1.2 g/cm^3. Parallelism at both ends of the sample was controlled within a tolerance of 0.2 mm. By observing the basic physical parameters of the coal sample (Table 1), it was found that the parameters of the quality, density and wave velocity of some selected samples had small differences, and the overall homogeneity of the coal sample was good.

Figure 3 shows the diagram of the experimental system, which mainly includes modules such as true triaxial loading, axial loading, impact loading and data acquisition. True triaxial and axial loading can successively apply triaxial unequal static prestress to a sample, and the dynamic load is controlled by the bullet launcher. The stress waveform of coal samples under true triaxial impact load can be captured and the mechanical characteristics of coal can be calculated and analyzed. The bullet, incident bar and transmission bar of this experimental device are all made of steel material, the rod diameter is 100 mm, the longitudinal wave propagation velocity (C) is 5100 m/s, and the elastic modulus (E) is 210 GPa.

Figure 4a displays the 3D unequal prestress loading device and the infrared velocimeter device in the experimental system. True triaxial cavity has a pressure system in three directions, which can apply effectively a specified amount of prestress to a sample. The three-way prestress is controlled by static loading control panel. Through infrared monitoring of the probe distance and the bullet through time, the impact speed of the impact process can be obtained. There is positive correlation between bullet impact velocity and dynamic load. Oil pumps in all directions can provide up to 30 MPa of prestress to a sample, and the dynamic load speed can reach over 20 m/s. Obviously, these loading devices can effectively achieve true triaxial and dynamic load failure experiments for coal samples at high strain rates.

Figure 4b displays the 3D prestress loading path of the experimental coal sample. Prestress was applied to a sample from the horizontal, vertical and axial directions in sequence, and the dynamic impact experiment was performed along the σ_x direction. In the experiment, different dynamic loads were applied to a coal sample by adjusting the impact pressure to impact the incident rod under different impact velocities.

Experimental Procedure

First, the sample was placed into the true triaxial cavity so that the sample was located in the specify location of the cavity. Then, prestress was applied on the sample by the loading system. The air compressor was used to provide the specified air power for the bullet launcher. Meanwhile, parameters of the infrared velocimeter and the strain test system were set. Next, the bullet was launched to impact the incident rod. Upon the completion of a set of experiment, the data were saved, and the sample was taken out to have its failure mode observed. In addition, for the uniaxial impact test, we used a high-speed camera to capture the dynamic impact failure process of coal samples in real time. The collection frame of the camera was set to 22000 frames. Coal samples were stored in sealed bags and then screened and weighed.

Some representative samples were also made into specific specimens for SEM testing. The SEM sample preparation process was as follows. (1) The fragments with relatively flat and clean surfaces were selected from some original and damaged specimens as the specimens to be scanned. (2) By cutting and pruning, the fragments were prepared into circular slices with a diameter of about 10 mm and a thickness of about 2–4 mm, which were used as observation samples. (3) A sample was glued to the sample table with conductive adhesive and a gold film was sprayed on the fracture surface, then the sample is placed on the test table. Subsequently, the fracture microstructure of coal samples was observed by scanning electron microscopy in laboratory. (4) The original morphology and fracture characteristics of fractured coal samples were observed by scanning electron microscopy, and then,

Table 1. Physical parameters of coal samples

No.	Weight (g)	Density (g/cm^3)	Wave velocity (km/s)
1	127.57	1.24	1.86
2	128.27	1.25	1.88
3	126.78	1.23	1.85
4	125.8	1.22	1.83
5	123.72	1.2	1.79
6	124.11	1.19	1.84
7	121.96	1.18	1.77
8	127.11	1.22	1.83
9	125.29	1.22	1.83
10	124.11	1.21	1.81
11	126.19	1.23	1.84
12	126.75	1.23	1.85
13	121.78	1.18	1.79
14	124.23	1.2	1.8

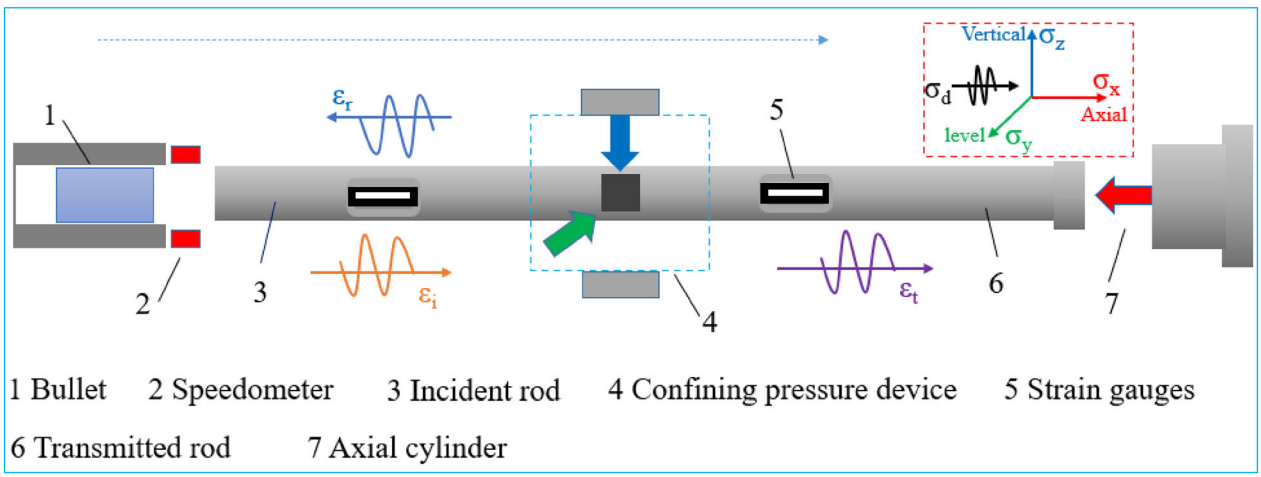

Figure 3. True triaxial experimental system.

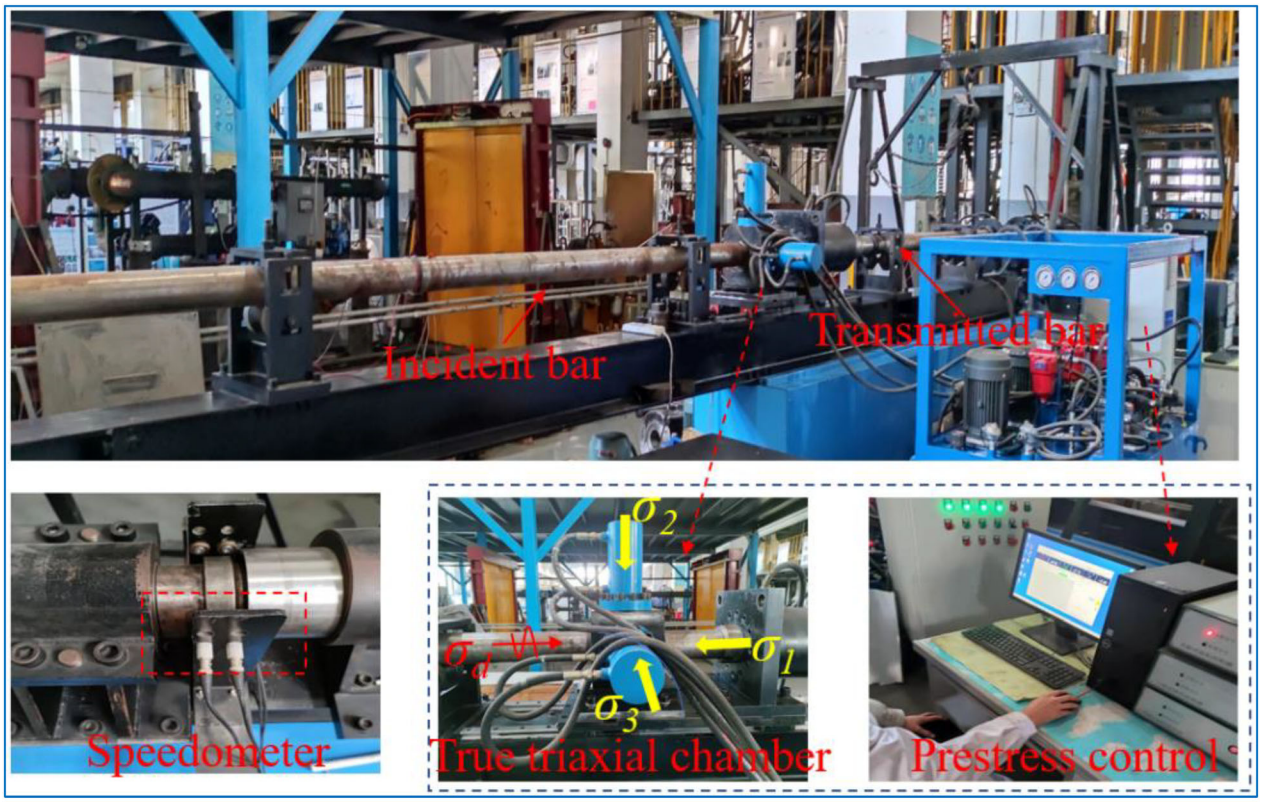

(a)

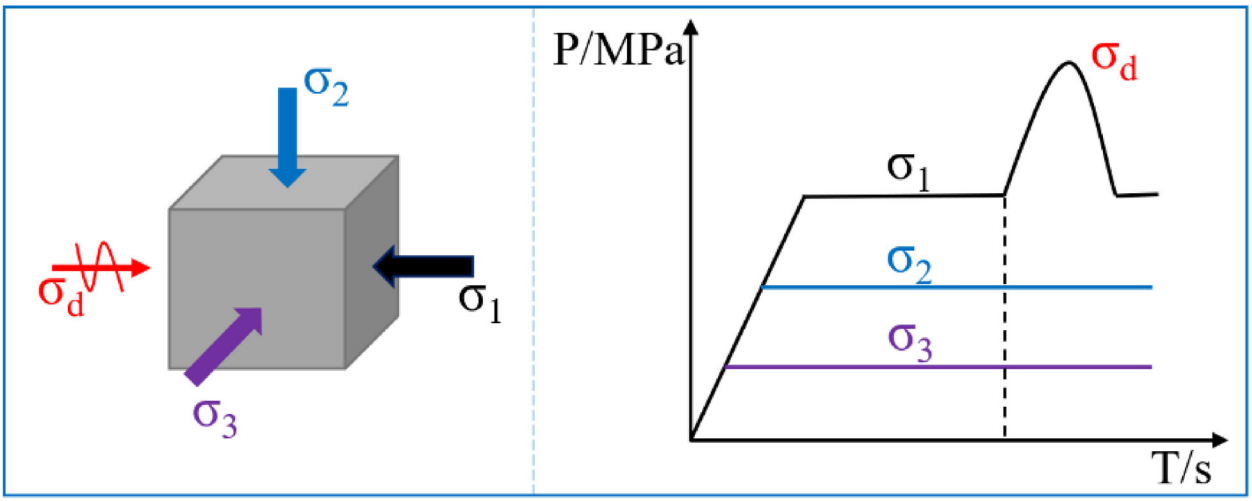

(b)

Figure 4. (**a**) Photographs of the experimental equipment. (**b**) Loading path of coal samples.

the cracking characteristics of coal samples induced by static prestress and dynamic load were analyzed.

Experimental Data Process

The stress wave formed by bullet impacting the incident rod will undergo multiple reflection and transmission propagations in the incident rod, sample and transmitted rod, thus forming the incident wave ε_{i}, the reflected wave ε_{r} and the transmitted wave ε_{t}. Based on the 1D elastic wave propagation theory (Liu et al. 2019), the stress at both ends along the axial direction of coal can be characterized as (Kong et al. 2021):

$$\begin{cases} P_1 = AE(\varepsilon_{\mathrm{i}} + \varepsilon_{\mathrm{r}}) + A_0\sigma_p \\ P_2 = AE\varepsilon_{\mathrm{t}} + A_0\sigma_p \end{cases} \tag{1}$$

where A and A_0 are, respectively, the cross-sectional area of the elastic bar and the sample; σ_{p} is axial static prestress of coal.

As the dynamic stress wave propagates along the axial direction and is applied to the coal sample, the velocities (V_1/V_2) ends of the coal sample are, respectively:

$$\begin{cases} v_1 = C(\varepsilon_i - \varepsilon_r) \\ v_2 = C\varepsilon_t \end{cases} \tag{2}$$

The displacements u_1 and u_2 of the two end faces of the specimen can be expressed as:

$$\begin{cases} u_1 = C\int_0^t (\varepsilon_i - \varepsilon_r)d_t \\ u_2 = C\int_0^t \varepsilon_t d_t \end{cases} \tag{3}$$

The average stress of the specimen can be calculated as follows (You et al. 2022a):

$$\sigma(t) + \sigma_p = \frac{P_1 + P_2}{2A_0} = \frac{A}{2A_0}E[\varepsilon_i(t) + \varepsilon_r(t) + \varepsilon_t(t)] + \frac{2A_0}{2A_0}\sigma_p \tag{4}$$

$$\sigma(t) = \frac{P_1 + P_2}{2A_0} = \frac{A}{2A_0}E[\varepsilon_i(t) + \varepsilon_r(t) + \varepsilon_t(t)] \tag{5}$$

Substituting Eq. 3 into Eq. 5, the average strain of the specimen can be calculated as:

$$\varepsilon(t) = \frac{u_1 - u_2}{L_0} = \frac{C}{L_0}\int_0^t [\varepsilon_i(t) - \varepsilon_r(t) - \varepsilon_t(t)]d_t \tag{6}$$

The strain rate can be obtained by differentiating this equation:

$$\dot{\varepsilon}_t = \frac{d\varepsilon(t)}{d_t} = \frac{C}{L_0}[\varepsilon_i(t) - \varepsilon_r(t) - \varepsilon_t(t)] \tag{7}$$

where L_0 is the sample length.

The stress and strain of coal samples were calculated according to the stress wave data collected in the experiment. At the same time, the morphology observation, fractal calculation and SEM tests of samples were carried out after impact. The mechanical properties of coal samples are discussed below comprehensively under three-way unequal prestress and different dynamic loads.

EXPERIMENTAL RESULTS

Stress Wave

As dynamic load acts on coal samples under different prestressed conditions, the stress wave curve is shown in Figure 5. The reflected waveform values were opposite to the incident and transmission directions. On the whole, there was a certain variation rule about the waveform amplitude under different axial static and dynamic loads. In Figure 5a, the amplitude of reflected wave and transmitted wave both increased first and then decreased with the increase in σ_1. The analysis showed that the increase in the static load made the fracture damage in coal sample aggravated gradually, leading to increase in wave impedance (Kong et al. 2021). In Figure 5b and c, the variation trend of stress wave shape was consistent. The amplitudes of incident wave, transmitted wave and reflected wave increased gradually. At the same impact velocity, the incident wave amplitude was larger than the reflected wave amplitude, while the reflected wave amplitude was much larger than the transmitted wave amplitude. It is believed that the increased impact velocity made the bullet gain more momentum to the impact the incident bar, prompting the incident wave amplitude to increase. When the incident wave passed forward to the contact area of coal, the impact of the reflection spread transmission amplitude value increased, but the stress wave gave priority to the reflection and this may be due to the impact of time was shorter. It is also related to the material property of the sample; that is, the porous microstructure in the coal. However, by comparing the transmitted wave amplitudes between the two figures, it was obvious that due to the provision of the three-way static prestress, the coal became

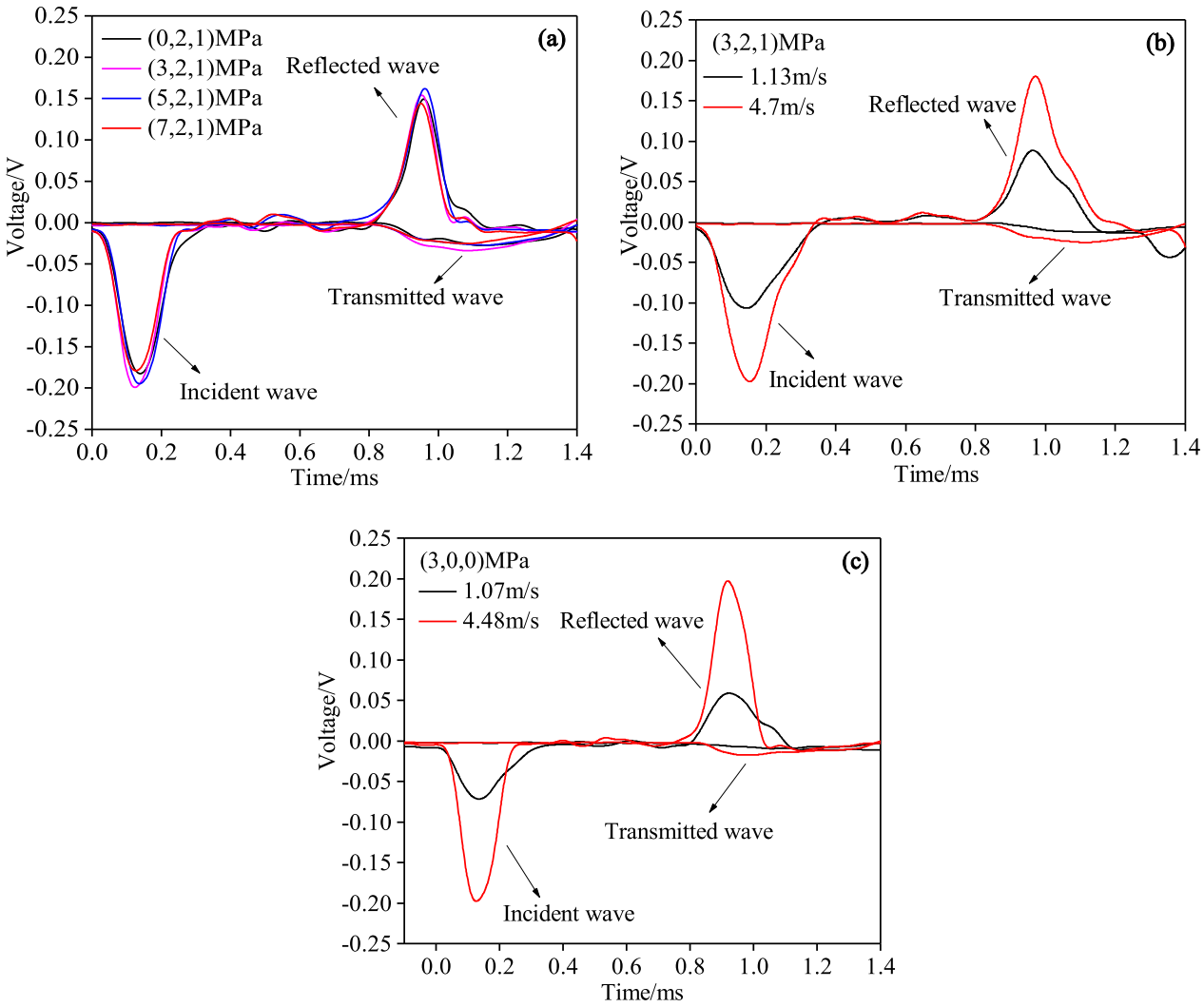

Figure 5. Stress wave curve.

denser, and more stress wave passed through the coal sample under true triaxial dynamic load. However, the original coal sample itself had many internal cracks and lacked the constraint of pre-stress, and so, less stress wave transmission passed through the coal.

Mechanical Curve

Figure 6 displays the dynamic curves of coal samples. Three parts can be described as the stress evolution process of coal: linear, plastic and failure stage. In the initial stage, the stress rose linearly with the increase in strain. Different from the conventional static stress curve (Liu et al. 2015; Li et al. 2021b; Ma et al. 2021, 2023), the initial compaction stage was not obvious in the dynamic curve. It is attributed to the following reason: Since the dynamic load did not last long under the impact load, the coal under the 3D prestresses was compacted quickly and then entered the linear stage. The micro-cracks expanded and new cracks were generated in the coal, thereby inducing damage with the coal sample from the linear stage into the plastic stage, and the stress soared to the peak stress with the increased strain. Meanwhile, the micro-cracks expanded further and the stress increased

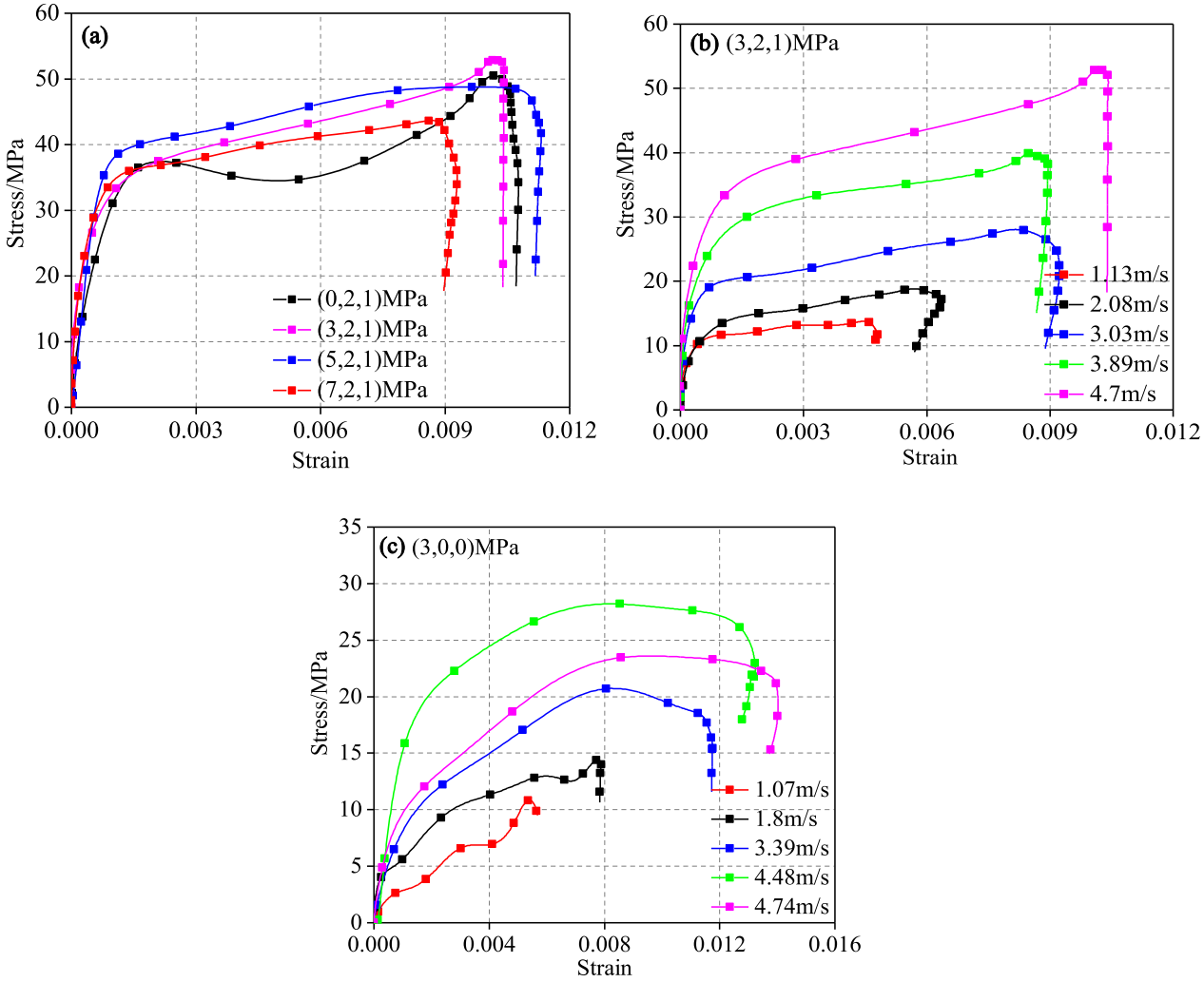

Figure 6. Dynamic curves of coal.

continuously. After the stress of coal reached the peak, stress decreased gradually due to damage or destruction of coal sample.

Failure Pattern

Figure 7 displays the macroscopic failure modes of coal samples under true triaxial impact, and that the overall modes of coal samples were intact. However, macroscopic cracks or slight edge shedding were observed on the surface of the coal. Damage occurred inside the coal sample and cracks occurred on the surface. Many small fragments were produced, and the whole was granular or powdery under the action of high load. Clearly, it was accompanied by intensified generation and expansion of micro-cracks with the increase in σ_1. Subsequently, the coal sample was damaged more severely.

As shown in Figure 8, the coal sample only produced cracks along the axial direction, and the whole sample basically contacted with the elastic rod without showing large area spalling or splashing when the impact velocity was 1.8 m/s. Part of the coal sample was split into large fragments and some small fragments when the impact velocity was 3.39 m/s. However, the coal sample was completely broken into fine particles when the impact velocities were 4.48 and 4.74 m/s. Therefore, under a low im-

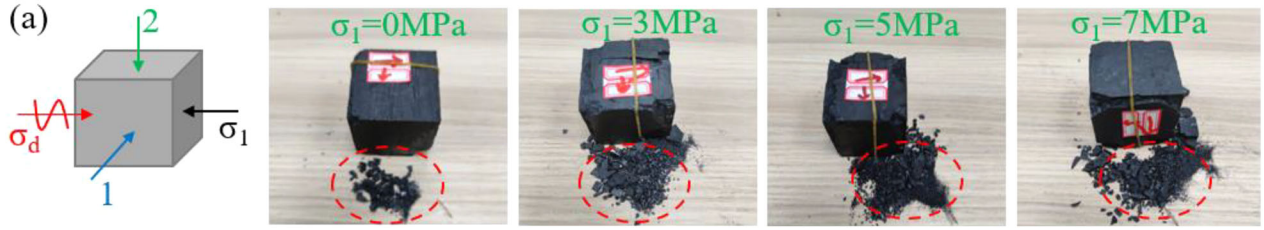

Figure 7. Macroscopic failure modes of true triaxial condition.

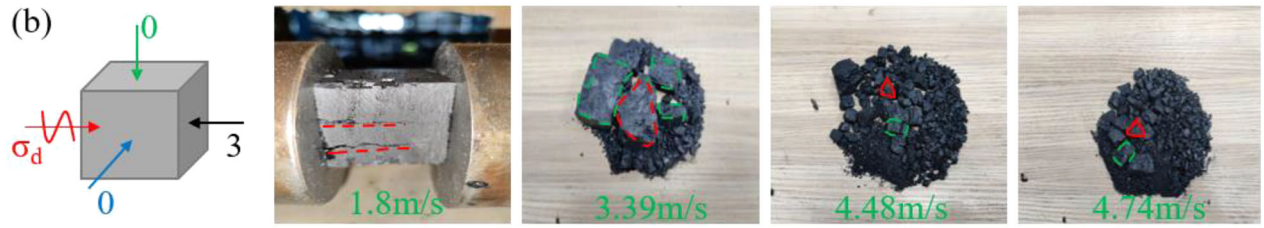

Figure 8. Macroscopic failure modes of true triaxial condition.

pact velocity, axial tensile cracks appeared in the coal sample, which experienced open and complete rupture; as the impact velocity rose, the sample was completely broken into blocks or particles. Based on the morphology of fragments under impact load, the destruction mode was mainly rectangular section, cone-shaped section fragments and wedge-shaped section fragments, showing the characteristics of crushing failure. The fragmentation degree of coal under true triaxial impact load was notably lower than that under uniaxial impact load, because the sample was constrained by 3D static load prestress.

ANALYSIS

Analysis of Coal Fracture Factors

Figure 9 shows the coal sample crushing process under uniaxial impact load, whereby the original micro-fracture in the coal body expanded and new cracks gradually occurred under dynamic load. The cracks generated along the axial impact direction, and the fracture cracks showed tensile failure as a whole. The lack of σ_2 and σ_3 forces resulted in a large number of fragments splash. The impact load continued until the crack of the sample was completely through and the coal sample was completely broken into fragments or granules.

In Figure 10, the overall shape is basically intact, and only each surface presented different forms of fracture. When the prestressed coal sample was (0,2,1) MPa, the shape of plane x of the coal was basically undamaged, and there were slight cracks in planes y and z. With the increase in axial static σ_1, the 3D stress difference of coal increased. The axial static load promoted the further expansion of the micro-cracks in the coal and aggravated the damage inside the coal. The x surface of the coal sample was still basically intact when the axial static load on the coal sample increased from 3 to 7 MPa. However, several cracks were generated in the y and z direction planes, and the cracks were at a certain angle to the axial direction, which was different from the overall axial propagation of the cracks in Figure 9. With the gradual increase in σ_1, the impact surface (x) of the coal sample was basically intact, while the surface constrained only by the prestress σ_2 and σ_3 had serious deformation and failure, especially the minimum principal stress surface (y). Therefore, the plane with the fastest stress unloading was prone to failure when it was impacted by a certain dynamic load when the difference of three-way prestress of coal rock increased.

Figure 11 shows the schematic diagram of under conventional triaxial (Kong et al. 2021). Coal samples were subjected to conventional confining pressure ($\sigma_2 = \sigma_3$). The crack propagation of coal

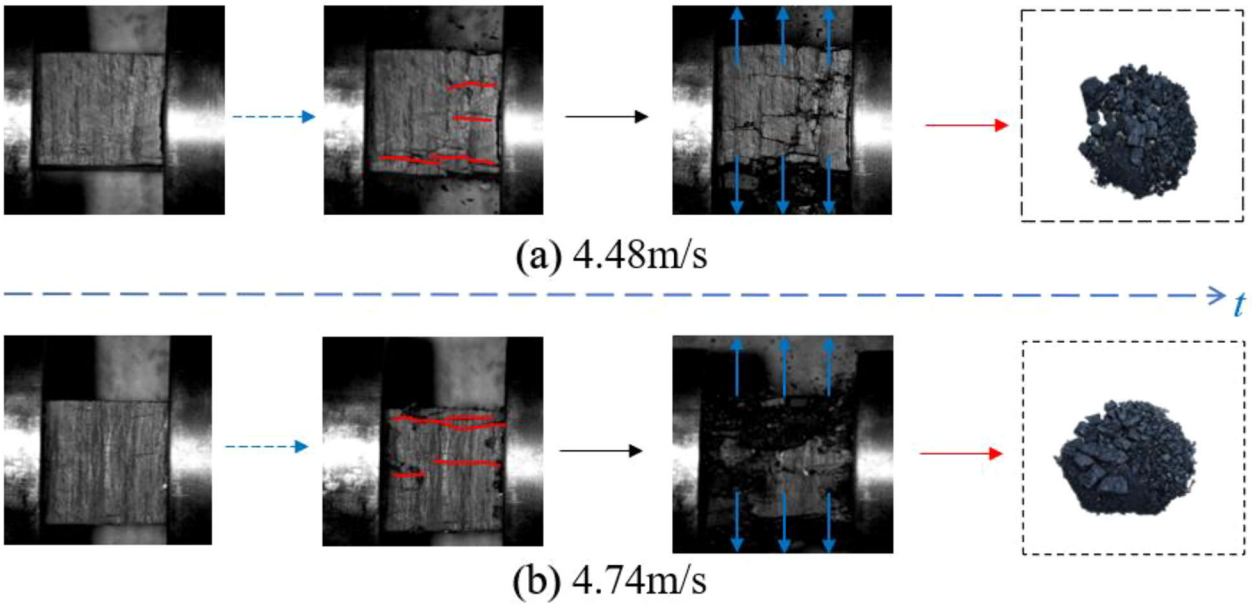

Figure 9. Fracture evolution under uniaxial impact.

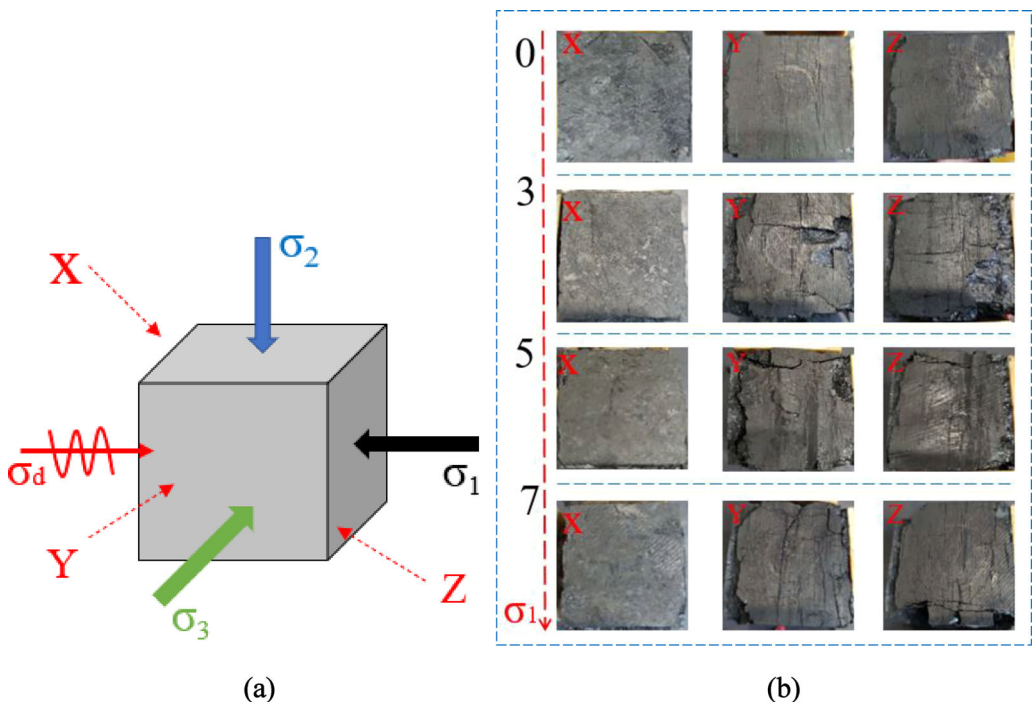

Figure 10. (**a**) Distribution of each plane of the coal. (**b**) Diagram of coal fracture surface under true triaxial loading.

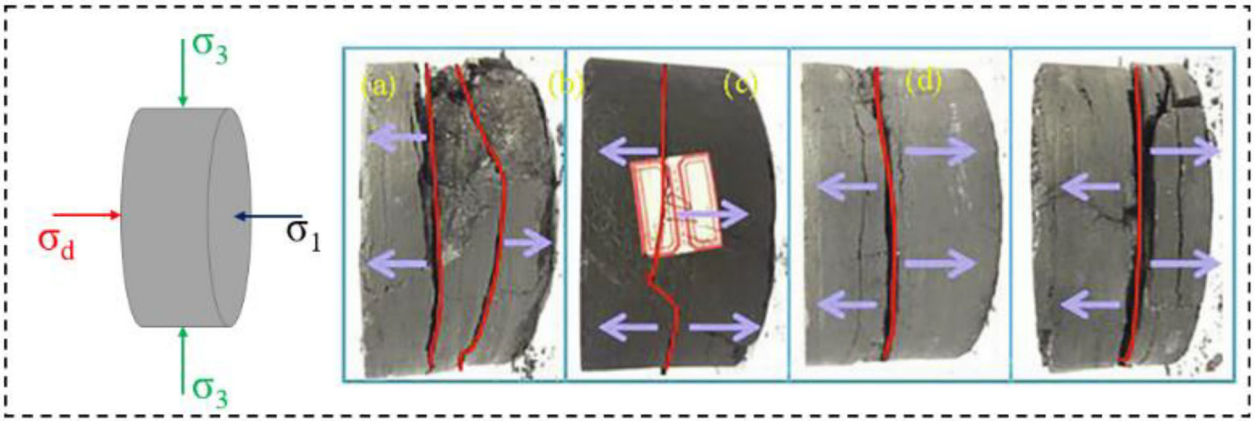

Figure 11. Failure diagram of coal under conventional confining pressure (Kong et al. 2021).

samples under dynamic load was basically perpendicular to the axial direction, and the analysis showed that the failure crack of coal body presented tensile failure (Kong et al. 2020). However, the force of coal studied in this paper was $\sigma_2 > \sigma_3$, and the circumferential force was uneven. The crack penetration direction was obviously different from that shown in Figure 11 after the coal was affected by the impact load. The fracture of the fracture plane contained more shear and tensile failure. This also fully reflected the anisotropic failure characteristics of coal samples under the action of true 3D. For the coal sample under uniaxial loading, the dynamic load along the axial direction played a major role in cracking due to the lack of lateral prestress. Although the coal samples constrained by the 3D prestress were subjected to the coupling action of axial and static loads, the lateral prestress effectively restricted the crack propagation of the coal, so that the cracks were not completely parallel to the axial direction and presented a certain angle.

Combined with the analysis of the macroscopic morphology of the sample broken in Figure 10, it is concluded that true 3D unequal prestress and dynamic load jointly acted on the coal sample. From Figure 12a, the cracks inside the coal sample were gradually compacted by external forces when the axial prestress was small. However, as the axial prestress continued to increase, the cracks and pores in the coal sample expanded along the fracture, and the bearing capacity of the coal sample decreased gradually. In Figure 12b, the provision of σ_2 and σ_3 made the crack denser to a certain extent and restricted the deformation of the coal. From Figure 12c, the dynamic load acted on the coal sample in a very short time, and the fracture continued were promoted to expand. Crack propagation of coal was intensified by the action of stress wave. Therefore, the combination of static prestress and dynamic impact force had a significant impact on the deformation of coal samples.

Analysis of Coal Failure Causes based on SEM

The cross section of coal after damage was detected by scanning electron microscope. As shown in Figure 13a–c, coal is a complex multi-fracture medium, the skeleton of the coal medium is composed of a large number of coal matrices (Zhou et al. 2023). There were a large number of cracks between the skeletons, and the original cracks were irregularly distributed. Based on the unique properties of coal itself, when the axial pressure σ_1 on coal body gradually increased, the coal sample gradually produced damage. When the stresses σ_2 and σ_3 were applied to the coal, they gradually become tight and restricted the deformation of the sample. Figure 13d–f shows the fracture morphology of coal under impact load. The fault zone runs through the middle of the coal body or between different crystal zone, and there is a slight dislocation on both sides. The grain boundary fracture was relatively smooth, and fractures or cracks occurred through the intact crystal, and the fracture was brittle fracture. In addition, there were some fragmentary particles attached to

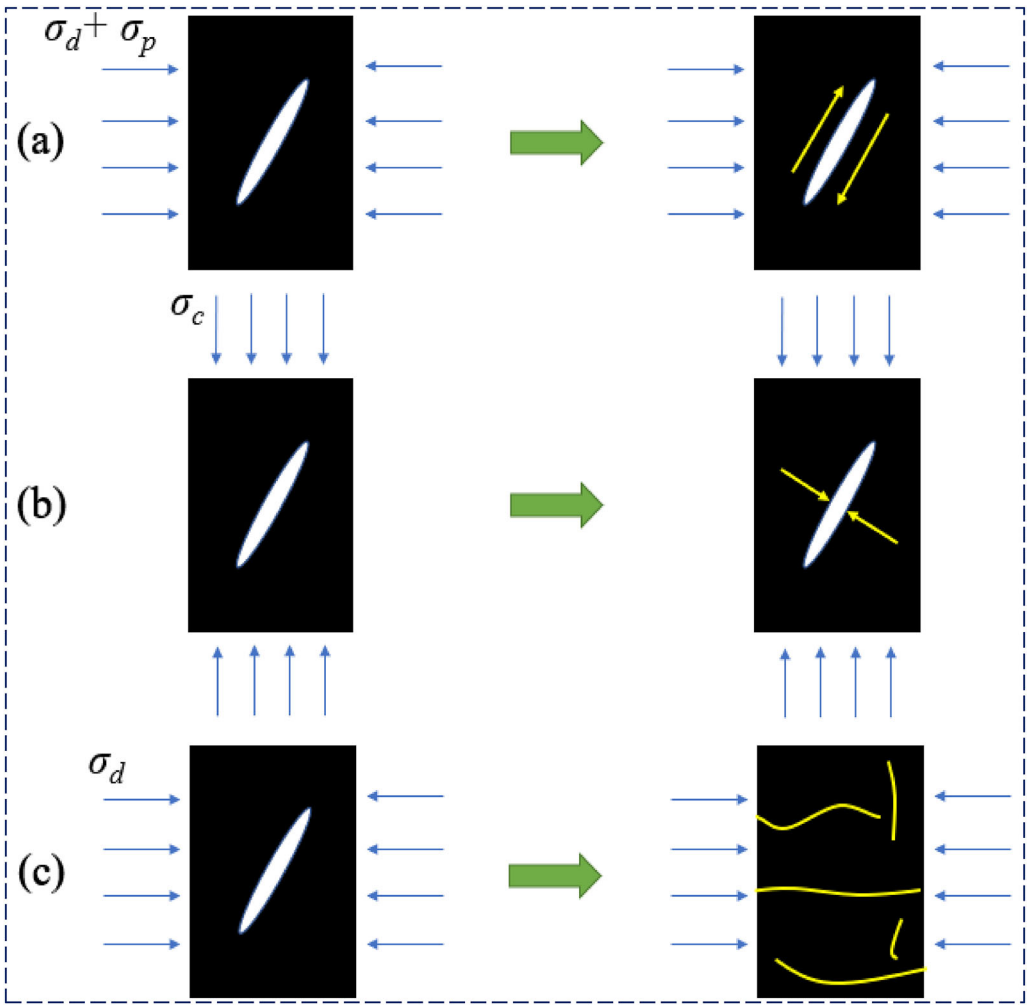

Figure 12. Effects of various factor on coal sample fracture.

the surface. When the stress wave contacted the fracture, it reflected into the tensile wave on the surface of the fracture and drove the crack to expand because of the many primary cracks in coal (Wang et al. 2021a; Gu et al. 2023b). According to the principle of fracture mechanics, when the stress wave loading these crack tip formed a stress concentration area, coal is destroyed since the tip can withstand limited plastic deformation (Wang et al. 2021b). Therefore, the stress wave imposed on coal was strengthened gradually, promoting the continuous penetration of primary cracks and new cracks, and the sample was broken gradually. This also better reflected the damage process of coal sample with macroscopic failure in Figure 8.

Analysis of Failure Characteristics of Coal Samples

Coal samples will produce fragments of different mass and size after failure, and so, it is necessary to quantitatively analyze the distribution characteristics of fragments. The debris of the specimen was treated by screening method (Shen et al. 2020; Chen et al. 2022). The screening sizes were > 45 mm, 31.5–45 mm, 22.4–31.5 mm, 7.1–22.4 mm, 1.7–7.1 mm, 0.5–1.7 mm, 0.1–0.5 mm, 0–0.1 mm, a total of eight grades. The mass percentage of fragments of different screening levels by weighing the fragments of different screening levels can be calculated as:

$$N = \frac{M_n}{M}\% \tag{8}$$

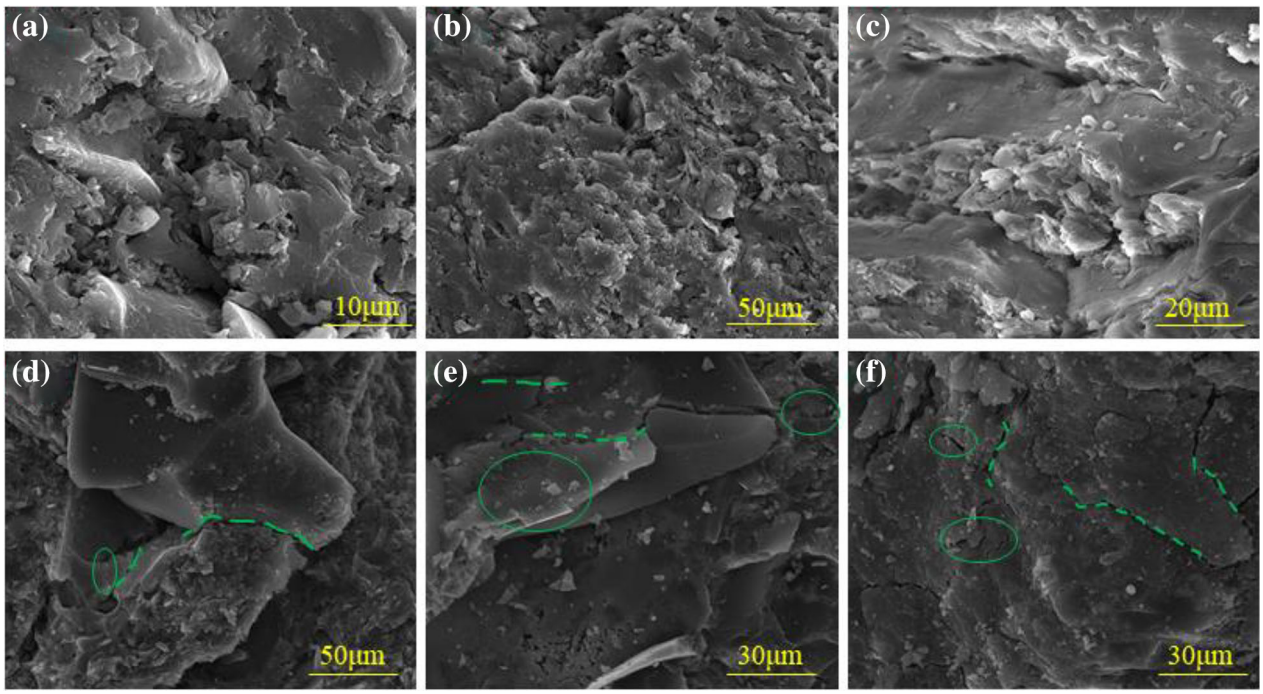

Figure 13. SEM image.

where *Mn* is the mass of fragments screened by two adjacent sieves. Different particle sizes correspond to different qualities of coal sample fragments under dynamic load. The fragment distribution of each sample after sieving is shown in Figure 14.

Figure 14a shows the broken sample diagram of coal. With the increase in σ_1, the fragments were mainly complete blocks, and the distribution of the fragments was relatively uniform. The fragments were mainly distributed in 45–47 mm, and then, the particle size of the fragments showed a rapid decline trend in the range of 7.1–22.4 mm. In addition to the complete fast-shaped broken samples, the rest were mainly granular or powder-like with a small particle size of 0.1–7.1 mm. The fragmentation quality of coal samples under (7,2,1) MPa in each section was higher than that under low prestress. Due to the existence of three-way static load prestress, the damage degree of coal samples was weaker than that under uniaxial impact, and no larger particles or larger fragments were produced. The fracture morphology of coal sample was mainly large chunks, followed by small particles.

In Figure 14b, when the impact velocity was 3.39 m/s, the maximum block size of the sample was distributed in 31.5–45 mm, and the minimum particle size was in the range of 0.1–0.5 mm. The maximum particle size distribution interval of the sample was 22.4–31.5 mm when the impact velocity was 3.89 and 4.48 m/s. Although the overall grain size change rule was the same as 3.39 m/s, the coal particle size in the smaller range was much higher than 3.39 m/s. The maximum particle size range of the fragments was 7.1–22.4 mm when the impact velocity was 4.84 m/s. This indicates that the fracture degree of coal samples was aggravated under the stress wave, and the samples evolved from intact form to massive form and then to granular form. According to the distribution of coal sample fragments, the quantitative characteristics were analyzed (Xie et al. 2000; Zhang et al. 2022). Due to the regularity of particle size distribution range after coal crushing, we considered using fractal dimension (Xie et al. 2000; Shen et al. 2022) for further analysis.

The fractal definition is generalized in the continuity and the form is (Xie et al. 2008):

$$N = Cr^{-D} \tag{9}$$

where r is the characteristic scale (particle size) of the object, N corresponds to the number of objects

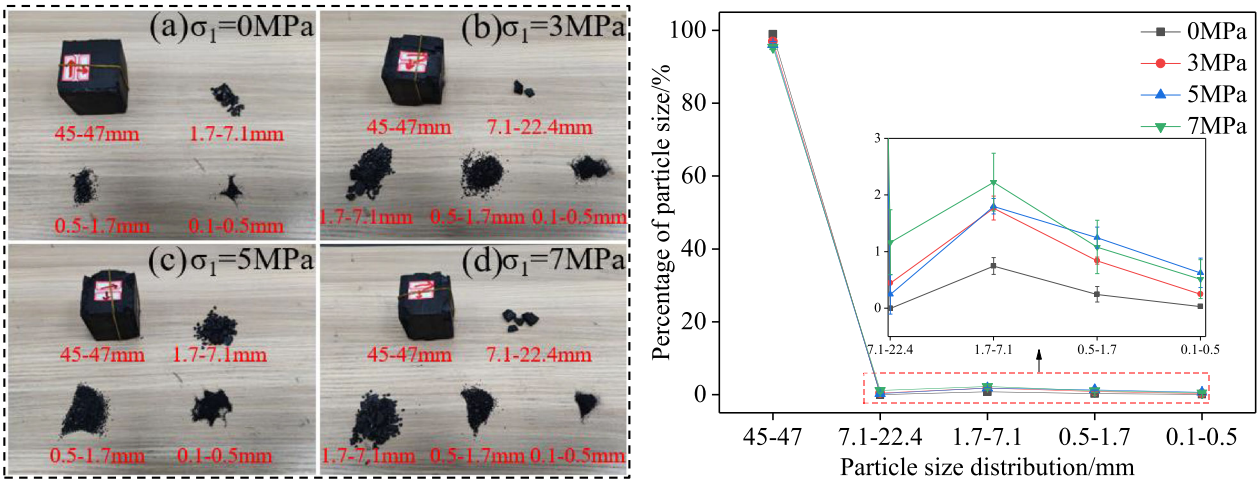

(a) Different coaxial static load ((σ1,2,1)MPa)

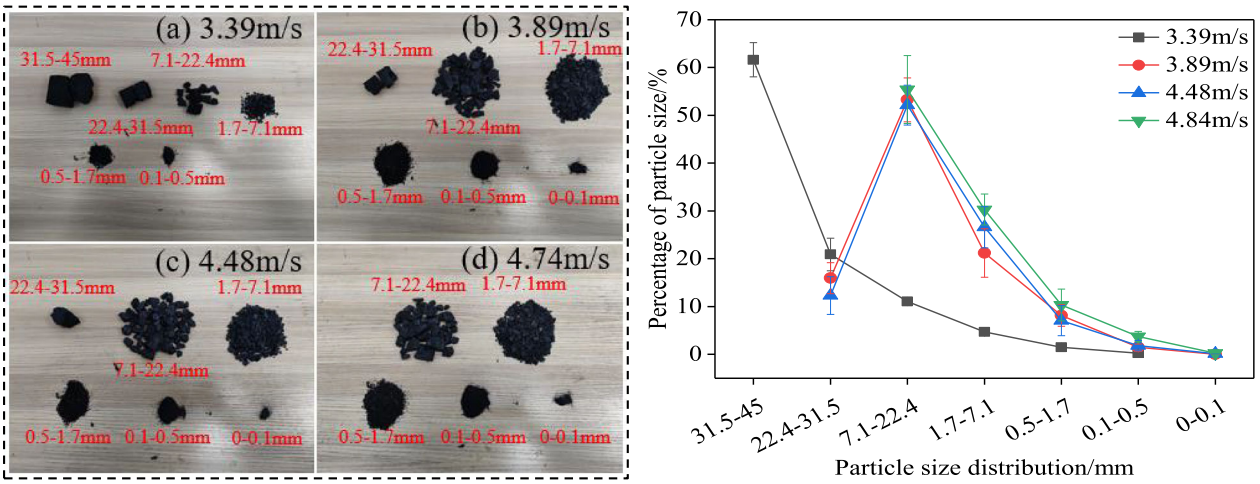

(b) Different impact velocity ((3,0,0)MPa)

Figure 14. Sample breakage distribution.

greater than or equal to r and C is the proportionality constant. The derivative of Eq. 9 is:

$$dN \propto r^{-D-1}dr \tag{10}$$

According to the mass–frequency relationship, the distribution equation of coal samples after failure is established as (Peng et al. 2015; Weng et al. 2019; Li et al.2020):

$$Y = M(r)/M = (r/r_m)^k \tag{11}$$

The derivative of Eq. 11 is:

$$dM \propto r^{k-1}dr \tag{12}$$

Combining Eqs. 11 and 12, we derive:

$$dM \propto r^3 dN \tag{13}$$

According to Eqs. 10, 12 and 13, the fractal dimension (D) of coal sample lumpiness distribution can be obtained as:

$$k = \lg[M(r)/M]/\lg(r) \tag{14}$$

$$D = 3 - k \tag{15}$$

where M is the total mass of debris, r is the equivalent particle size, namely the screen diameter.

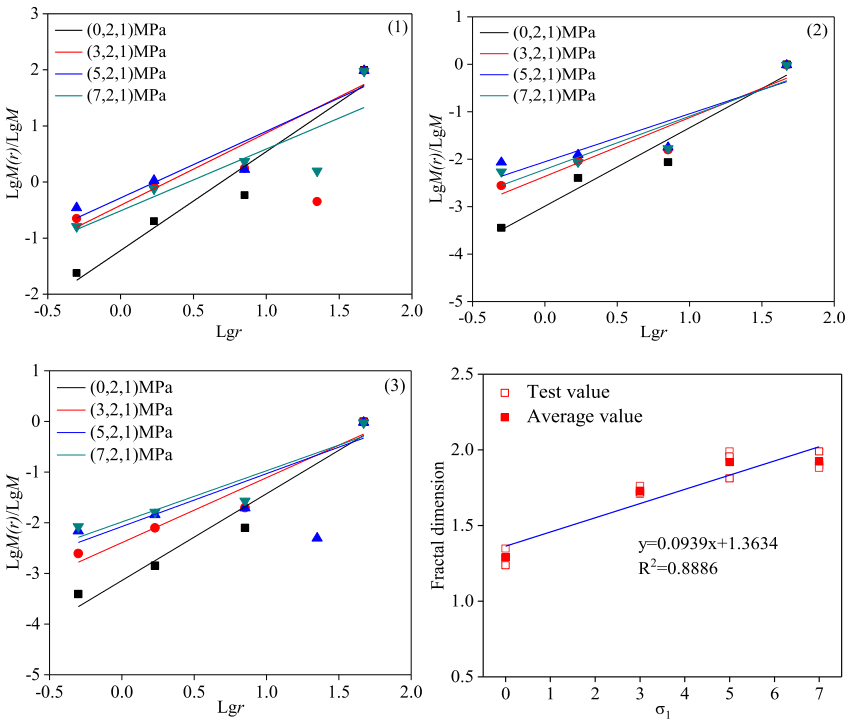

(a) Fractal dimension under different axial load σ_1

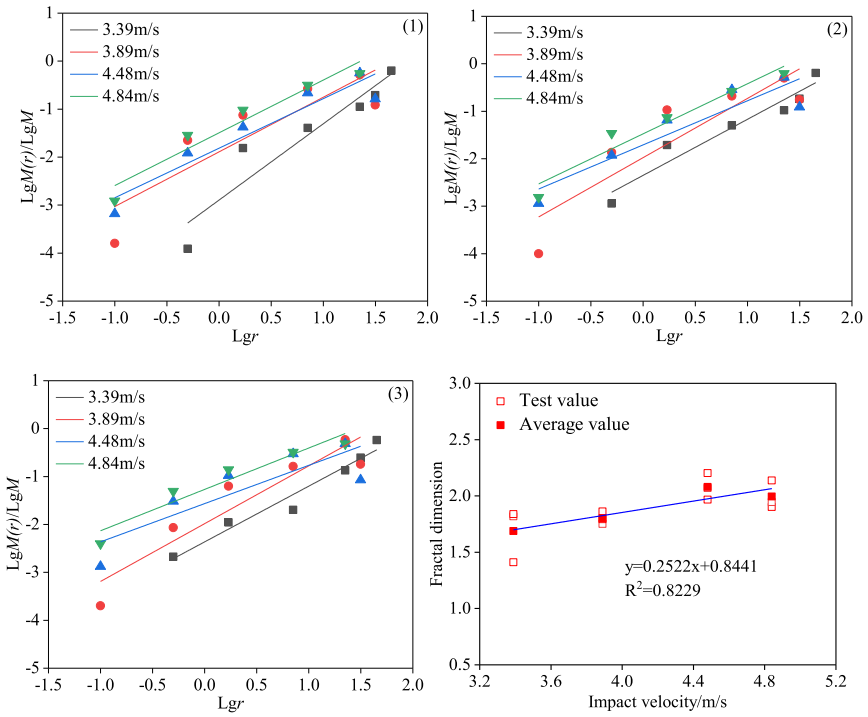

(b) Fractal dimension under different impact velocity

Figure 15. Fractal dimension of coal fragmentation.

Figure 15a shows the fractal law of coal failure under the change of σ_1. D increased gradually with the increase in σ_1. The D and σ_1 can be expressed as:

$$D = 0.0939\sigma_1 + 1.3634 \tag{16}$$

Equation 16 shows that the increase in σ_1 gradually aggravates the damage inside the coal when σ_2 and σ_3 remain unchanged. With the action of dynamic load, the coupling effect of static load and dynamic load made the coal sample breakage worse. Figure 15b shows the fractal curve of coal under different impact velocities ((3,0,0) MPa). The relationship between the fractal dimension D and the impact velocity v can be expressed as:

$$D = 0.2522v + 0.8441 \tag{17}$$

The fractal dimension D increases linearly with impact velocity. When the impact velocity was 3.39 m/s, the fractal dimension was small, and the specimen contains larger particles. The fractal dimension was large and the sample was broken seriously when the dynamic load of the coal sample increased. Therefore, the fractal dimension of the specimen increased gradually and the specimen was broken seriously when the dynamic load stress wave increased.

DISCUSSION

Stress and Failure Evolution

Based on the evolution law of stress obtained in this paper, combined with the energy and failure characteristics of coal samples, the dynamic evolution characteristics of coal under different prestress conditions were analyzed. Following the principle of 1D stress wave, incident energy (W_i), reflected energy (W_r) and transmitted energy (W_t) (Wang et al. 2021c; Li et al. 2023d) about dynamic action on coal were defined in dynamic impact process (Zang et al. 2021; You et al. 2022b):

$$\begin{cases} W_{\mathrm{i}} = \frac{AC}{E}\int \sigma_i(t)^2 d_t \\ W_{\mathrm{r}} = \frac{AC}{E}\int \sigma_r(t)^2 d_t \\ W_{\mathrm{t}} = \frac{AC}{E}\int \sigma_t(t)^2 d_t \end{cases} \tag{18}$$

Referring to the relevant triaxial Hopkinson impact experimental research literature (Zhu et al.2021; Wu et al. 2022), the absorbed energy of coal under the process of impact can be expressed as:

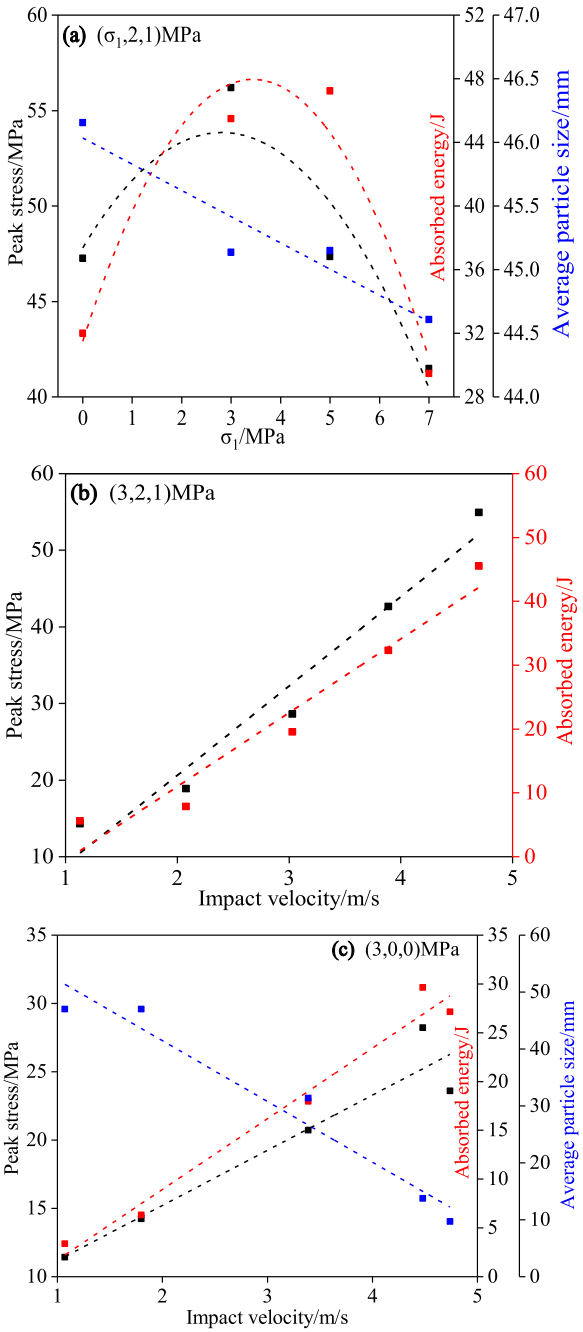

Figure 16. Relationship between stress and energy and particle size.

$$w_{\mathrm{a}} = w_{\mathrm{i}} - w_{\mathrm{r}} - w_{\mathrm{t}} \tag{19}$$

Quantitative characterization of coal failure samples under different static load prestresses and impact velocities was carried out. The average par-

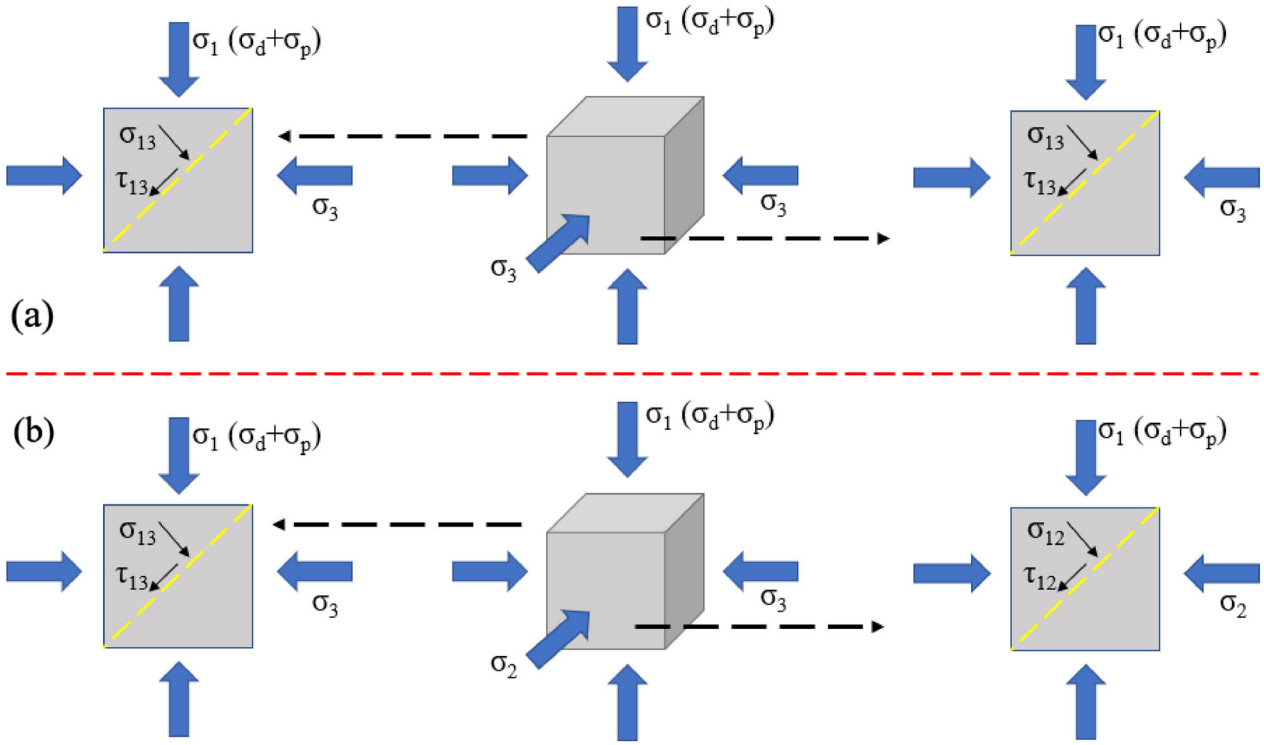

Figure 17. Stress state of coal sample.

ticle size was calculated by counting the broken sample mass obtained by sieve screening (Tian et al. 2023):

$$D = \frac{M_1 D_1 + M_2 D_2 + \cdots + M_n D_{\mathrm{n}}}{M} \tag{20}$$

where D_{n} is the average value of the mesh holes of the corresponding two sieves.

As shown in Figure 16a, keeping the prestresses σ_2 and σ_3 unchanged, the peak stress intensity, average particle size and absorbed energy consumption of coal decreased gradually with the increase in σ_1. Obviously, the difference of three-way prestress increased. The internal cracks of coal samples ran through and developed, the distribution was crisscross, the structural damage was large, and more serious damage occurred. The compressive strength of coal was reduced, and the energy consumption required for dynamic impact was reduced. In Figure 16b and c, the peak stress intensity and absorption energy of coal increased gradually with the increase in dynamic load, and the average particle size of crushing decreased gradually. The increase in the impact velocity strengthened the stress wave acting on coal body and promoted the continuous coalescence of primary and new fractures. The sample was broken gradually and the average particle size decreased gradually, while the large amount of coal crushing required more energy. At the same time, the mechanical strength of coal under (3,2,1) MPa was higher than that under (3,0,0) MPa, and the three-way static load prestress also increased the mechanical strength of coal to a certain extent.

Influence Factors of Prestress and Dynamic Load on Coal Sample

Based on the analysis of some mechanical data mentioned above, the mechanical strength of coal samples under three-way prestressing is significantly improved compared with that under uniaxial impact. As is known to all, scholars (e.g., Kong et al. 2021) have shown that in conventional triaxial experiments ($\sigma_2 = \sigma_3$), the dynamic strength increased greatly with σ_3. As shown in Figure 17a, the crack opening

in the lateral direction of the sample was limited due to the confining pressure σ_3, and the crack cannot propagate and required a larger shear force (Kong et al. 2018). The effective shear force for crack propagation and initiation is defined as:

$$\tau_{\text{eff}} = |\tau_{13}| - \sigma_{13} \cdot \tan\varphi = \frac{\sigma_1 - \sigma_3}{2\cos\varphi} - \frac{\sigma_1 + \sigma_3}{2}\tan\varphi \tag{21}$$

$$\tau_{\text{eff}} = \frac{(\sigma_d + \sigma_p) - \sigma_3}{2\cos\varphi} - \frac{(\sigma_d + \sigma_p) + \sigma_3}{2}\tan\varphi \tag{22}$$

According to Eq. 22, coal sample failure required high shear force, which fully indicates that confining pressure promoted the increase in the mechanical strength of coal and rock.

In this study, true triaxial compression test ($\sigma_2 \neq \sigma_3$) has been carried out on coal. In Figure 8, coal deformation under true triaxial state was limited relative to uniaxial impact, and the mechanical strength of coal under true triaxial prestressed state was greater. Relevant literature also showed that, with the increase in σ_2, the mechanical strength of coal mass increased (Liu et al. 2021; Gu et al. 2023a, 2023b). With the provision of σ_2, the inhibition increased sharply. This shows that crack propagation was also inhibited in the σ_2 plane.

Based on the analysis of shear stress under conventional confining pressure σ_3, the effective shear stress τ_{eff} of σ_2 plane is expressed as (Kong et al. 2018):

$$\tau_{\text{eff}} = |\tau_{12}| - \sigma_{12} \bullet \tan\varphi = \frac{\sigma_1 - \sigma_2}{2\cos\varphi} - \frac{\sigma_1 + \sigma_2}{2}\tan\varphi \tag{23}$$

$$\tau_{\text{eff}} = \frac{(\sigma_d + \sigma_p) - \sigma_2}{2\cos\varphi} - \frac{(\sigma_d + \sigma_p) + \sigma_2}{2}\tan\varphi \tag{24}$$

According the Eq. 24 and the principle of mechanical strength rising under conventional confining pressure σ_3, the σ_2-plane micro-crack propagation required a higher σ_1 ($\sigma_d + \sigma_P$). Therefore, the mechanical strength increased under certain σ_2 and σ_3, and coal failure occurred when reaching the critical shear strain energy.

With continuous increase in the axial prestress, static load promoted the damage of coal sample, and the internal crack was derived and expanded. With a certain confining pressure provided, crack propagation of coal samples was gradually limited. When the static load caused great damage to the coal sample, only a small dynamic load can cause the coal to fail. However, when the coal was subjected to a small static load σ_1 and lateral binding force of σ_2 and σ_3 was enough to limit the deformation of the coal sample, a larger dynamic load was needed to produce rupture. In relevant literature, it was proposed that total stress σ_1 should include static prestress σ_p and dynamic prestress σ_d, and the total stress can be expressed as:

$$\sigma_{\text{total}} = \sigma_p + \sigma_d \tag{25}$$

You et al. (2022a) studied the total stress of rock in 3D state basically remains unchanged with the increase in axial static load. However, the total strengths of coal samples in the study at 0, 3, 5 and 7 MPa were 47.26, 59.2, 52.34 and 48.47 MPa; thus, the strength was first increasing and then decreasing. Obviously, compared with rock samples, coal samples are more sensitive under axial static load. The failure of coal sample under high axial static prestress did not require too high dynamic load. Zhou et al. (2022) studied that the total strength of rock increased gradually with the increase in axial pressure. Since the total mechanical strength in this study was a parameter of the final breaking of rock under repeated impact, it may be related to providing a small dynamic load. This also proved that the dynamic load also played a key role in the coal sample after the coal sample is subjected to static load. When the static load was not enough to damage or destroy the coal sample, higher dynamic load was required. The analysis of total stress will be further studied in the future, whether there is a certain ultimate total strength under static load and dynamic load.

Other Factors

Compared with the relevant literature, rock and concrete samples presented shear failure under true triaxial conditions. Coal, as a kind of semi-hard brittle rock with many fractures, is an anisotropic heterogeneous medium, and there are some differences in physical and mechanical properties between coal and rock. Moreover, primary cracks on the surface of a coal sample may continue to expand due

to the action of dynamic load, and so, the coal sample presented mixed shear or tensile failure. The microstructure and internal composition of the sample also had a certain impact on its mechanical properties. In the future, true triaxial mechanical impact experiments will continue to be carried out for coal samples under different bedding and water content, and the evolution process of crack growth under true triaxial constraints of coal samples can be retrieved by means of acoustic emission devices, CT tests and numerical simulation (Liu et al. 2022; Wang et al. 2022b; Yang et al. 2023; Zang et al. 2023; Ding et al. 2023).

Therefore, for deep underground engineering protection, in order to prevent the occurrence of dynamic disasters, measures can be taken from the following aspects. That is, pay attention to monitoring the three-way stress to prevent that the three-way stress difference from becoming too large, that is, to reasonably control the mining speed while reducing the underground blasting and other dynamic load.

CONCLUSIONS

The transmitted amplitude of coal sample decreases with the increase in σ_1, indicating that the increase in the axial load aggravates the damage of coal sample. Under uniaxial and true triaxial conditions, the transmitted wave amplitudes increase with the increase in impact velocity, indicating that the increase in the impact velocity causes more stress waves to pass through the coal sample.

The peak strength of coal samples decreases gradually with the increase in σ_1 and increases with the increase in impact velocity under true triaxial conditions. Compared with uniaxial impact, the mechanical strength of coal sample under true triaxial impact increases significantly.

The absorbed energy of the coal sample decreases with the increase in σ_1 and increases with the increase in impact velocity. With the increase in σ_1 and impact velocity, the average particle size of the broken samples decreases gradually, and the fractal dimension increases with the increase in σ_1 and impact velocity.

The gradual increase in the axial compression σ_1 causes the coal to slide along the cross section, and the increase in the confining pressures σ_2 and σ_3 limits the deformation of the coal. Dynamic load is the main factor leading to coal cracking and continuous crack propagation.

ACKNOWLEDGMENTS

We gratefully acknowledge the financial support for this work provided by the Postgraduate Research & Practice Innovation Program of Jiangsu Province (KYCX23_2843), the Graduate Innovation Program of China University of Mining and Technology (2023WLKXJ133), the National Natural Science Foundation of China (52074276) and the National project funding for Key R&D programs of China (2022YFC3004702).

DECLARATIONS

Conflict of Interest The authors declare that there is no conflict of interest regarding the publication of this paper.

REFERENCES

Chen, M. D., Xu, S. L., Yuan, L. Z., Miao, C. H., Lu, J. H., Ma, H., & Wang, P. F. (2023). Influence of stress state on dynamic behaviors of concrete under true triaxial confinements. *International Journal of Mechanical Sciences, 253*, 108399.

Chen, R., Yao, W., Lu, F., & Xia, K. (2018). Evaluation of the stress equilibrium condition in axially constrained triaxial SHPB tests. *Experimental Mechanics, 58*(3), 527–531.

Chen, S., Zhang, H., Wang, L., Yuan, C., Meng, X., Yang, G., & Lu, Y. (2022). Experimental study on the impact disturbance damage of weakly cemented rock based on fractal characteristics and energy dissipation regulation. *Theoretical and Applied Fracture Mechanics, 122*, 103665.

Ding, Z., Feng, X. J., Wang, E. Y., Wei, Q. L., Zhao, X., & Hu, Q. J. (2023). Acoustic emission response and evolution of pre-cracked coal in the meta-instability stage under graded loading. *Engineering Geology, 312*, 106930.

Du, H. B., Dai, F., Wei, M. D., Li, A., & Yan, Z. L. (2021). Dynamic compression-shear response and failure criterion of rocks with hydrostatic confining pressure: An experimental investigation. *Rock Mechanics and Rock Engineering, 54*(2), 955–971.

Duan, M. K., Jiang, C. B., Yin, W. M., Yang, K., Li, J. Z., & Liu, Q. J. (2021). Experimental study on mechanical and damage characteristics of coal under true triaxial cyclic disturbance. *Engineering Geology, 295*, 106445.

Feng, X. J., Ding, Z., Ju, Y. Q., Zhang, Q. M., & Ali, M. (2022). ''Double Peak'' of dynamic strengths and acoustic emission responses of coal masses under dynamic loading. *Natural Resources Research, 31*(3), 1705–1720.

Gong, H. L., Luo, Y. X., Zhou, J. R., Zhao, C. C., & Li, X. P. (2023). Fracture behaviors and damage evolution anisotropy of granite under coupling of multiaxial confinement and dy-

namic loading. *Rock Mechanics and Rock Engineering, 56*(4), 2515–2534.
Grote, D. L., Park, S. W., & Zhou, M. (2001). Dynamic behavior of concrete at high strain rates and pressures: I. experimental characterization. *International Journal of Impact Engineering, 25*(9), 869–886.
Gu, Z. J., Shen, R. X., Liu, Z. T., Zhao, E. L., Chen, H. L., Yuan, Z. C., & Tian, J. W. (2023b). Dynamic characteristics of coal under triaxial constraints based on the split-hopkinson pressure bar test system. *Natural Resources Research, 32*(2), 587–601.
Gu, Z., Shen, R., Liu, Z., Zhou, X., Li, X., Zang, Z., & Wang, X. (2023a). Strain rate effect and mechanical constitutive model of coal samples under dynamic load. *Natural Resources Research*. https://doi.org/10.1007/s11053-023-10247-8.
He, M. C., Sousa, L. R. E., Miranda, T., & Zhu, G. L. (2015). Rockburst laboratory tests database - Application of data mining techniques. *Engineering Geology, 185*, 116–130.
Hu, W. R., Liu, K., Potyondy, D. O., & Zhang, Q. B. (2020). 3D continuum-discrete coupled modelling of triaxial Hopkinson bar tests on rock under multiaxial static-dynamic loads. *International Journal of Rock Mechanics and Mining Sciences, 134*, 104448.
Huang, B. F., Fu, S., & Xiao, Y. (2021). Uniaxial compressive behavior of granite at high strain rates. *Rock Mechanics and Rock Engineering, 54*(9), 4695–4721.
Ji, D. L., Zhao, H. B., & Vanapalli, S. K. (2023). Damage evolution and failure mechanism of coal sample induced by impact loading under different constraints. *Natural Resources Research, 32*(2), 619–647.
Kong, R., Feng, X. T., Zhang, X. W., & Yang, C. X. (2018). Study on crack initiation and damage stress in sandstone under true triaxial compression. *International Journal of Rock Mechanics and Mining Sciences, 106*, 117–123.
Kong, X. G., Li, S. G., Wang, E. Y., Ji, P. F., Wang, X., Shuang, H. Q., & Zhou, Y. X. (2021). Dynamics behaviour of gas-bearing coal subjected to SHPB tests. *Composite Structures, 256*, 113088.
Kong, X. G., Wang, E. Y., Li, S. G., Lin, H. F., Zhang, Z. B., & Ju, Y. Q. (2020). Dynamic mechanical characteristics and fracture mechanism of gas-bearing coal based on SHPB experiments. *Theoretical and Applied Fracture Mechanics, 105*, 102395.
Li, B. L., Wang, E. Y., Li, Z. H., Cao, X., Liu, X. F., & Zhang, M. (2023a). Automatic recognition of effective and interference signals based on machine learning: A case study of acoustic emission and electromagnetic radiation. *International Journal of Rock Mechanics and Mining Sciences, 170*, 105505.
Li, C. J., Xu, Y., Chen, P. Y., Li, H. L., & Lou, P. J. (2020). Dynamic mechanical properties and fragment fractal characteristics of fractured coal-rock-like combined bodies in split hopkinson pressure bar tests. *Natural Resources Research, 29*(5), 3179–3195.
Li, H. R., He, M. C., Qiao, Y. F., Cheng, T., Xiao, Y. M., & Gu, Z. J. (2023d). Mode I fracture properties and energy partitioning of sandstone under coupled static-dynamic loading: Implications for rockburst. *Theoretical and Applied Fracture Mechanics, 127*, 104025.
Li, H. R., Qiao, Y. F., He, M. C., Shen, R. X., Gu, Z. J., Cheng, T., & Tang, J. (2023b). Effect of water saturation on dynamic behavior of sandstone after wetting-drying cycles. *Engineering Geology, 319*, 107105.
Li, H. R., Qiao, Y. F., Shen, R. X., He, M. C., Cheng, T., Xiao, Y. M., & Tang, J. (2021b). Effect of water on mechanical behavior and acoustic emission response of sandstone during loading process: Phenomenon and mechanism. *Engineering Geology, 294*, 106386.
Li, T. R., Li, G., Ding, Y. Q., Kong, T. Q., Liu, J. G., Zhang, G. K., & Zhang, N. (2022). Impact response of unsaturated sandy soil under triaxial stress. *International Journal of Impact Engineering, 160*, 104062.
Li, X. F., Li, H. B., Zhang, Q. B., Jiang, J. L., & Zhao, J. (2018). Dynamic fragmentation of rock material: Characteristic size, fragment distribution and pulverization law. *Engineering Fracture Mechanics, 199*, 739–759.
Li, X. L., Liu, Z. T., Feng, X. J., Zhang, H. J., & Feng, J. J. (2021a). Effects of acid sulfate and chloride ion on the pore structure and mechanical properties of sandstone under dynamic loading. *Rock Mechanics and Rock Engineering, 54*(12), 6105–6121.
Li, X., Liu, Z., Zhao, E., Liu, Y., Feng, X., & Gu, Z. (2023c). Experimental study on the damage evolution behavior of coal under dynamic brazilian splitting tests based on the split hopkinson pressure bar and the digital image correlation. *Natural Resources Research, 32*(3), 1435–1457.
Liu, D. Q., Zhang, S. D., He, P. F., He, M. C., & Kulatilake, P. H. S. W. (2021). Experimental research on mechanical behaviors of the cubic jointed coal mass subjected to the true triaxial stress. *Journal of China University of Mining & Technology, 50*, 115–122. in Chinese.
Liu, K., Zhang, Q. B., Wu, G., Li, J. C., & Zhao, J. (2019). Dynamic mechanical and fracture behaviour of sandstone under multiaxial loads using a triaxial hopkinson bar. *Rock Mechanics and Rock Engineering, 52*(7), 2175–2195.
Liu, K., Zhao, J., Wu, G., Maksimenko, A., Haque, A., & Zhang, Q. B. (2020b). Dynamic strength and failure modes of sandstone under biaxial compression. *International Journal of Rock Mechanics and Mining Sciences, 128*, 104260.
Liu, P. F., Liu, K., & Zhang, Q. B. (2020a). Experimental characterisation of mechanical behaviour of concrete-like materials under multiaxial confinement and high strain rate. *Construction and Building Materials, 258*, 119638.
Liu, X. H., Dai, F., Zhang, R., & Liu, J. F. (2015). Static and dynamic uniaxial compression tests on coal rock considering the bedding directivity. *Environmental Earth Sciences, 73*(10), 5933–5949.
Liu, Y. B., Lebedev, M., Zhang, Y. H., Wang, E. Y., Li, W. P., Liang, J. B., & Ma, R. P. (2022). Micro-cleat and permeability evolution of anisotropic coal during directional CO2 flooding: An in situ micro-CT study. *Natural Resources Research, 31*(5), 2805–2818.
Liu, Y. B., Wang, E. Y., Jiang, C. B., Zhang, D. M., Li, M. H., Yu, B. C., & Zhao, D. (2023). True triaxial experimental study of anisotropic mechanical behavior and permeability evolution of initially fractured coal. *Natural Resources Research, 32*(2), 567–585.
Luo, Y., Gong, H. L., Huang, J. H., Wang, G., Li, X. P., & Wan, S. (2022). Dynamic cumulative damage characteristics of deep-buried granite from Shuangjiangkou hydropower station under true triaxial constraint. *International Journal of Impact Engineering, 165*, 104215.
Ma, H. F., Song, Y. Q., Chen, S. J., Yin, D. W., Zheng, J. J., Shen, F. X., & Ma, Q. (2021). Experimental investigation on the mechanical behavior and damage evolution mechanism of water-immersed gypsum rock. *Rock Mechanics and Rock Engineering, 54*(9), 4929–4948.
Ma, H. F., Song, Y. Q., Yang, J. K., Zheng, J. J., Shen, F. X., Shao, Z. X., & Xia, Z. G. (2023). Experimental investigation on physical-mechanical behaviors and macro-micro-structural responses of lignite subjected to freeze-thaw cycles. *Natural Resources Research, 32*(2), 543–566.
Peng, R. D., Ju, Y., Wang, J. G., Xie, H. P., Gao, F., & Mao, L. T. (2015). Energy dissipation and release during coal failure under conventional triaxial compression. *Rock Mechanics and Rock Engineering, 48*(2), 509–526.
Shen, Y., Shen, X., Liu, H. L., Ge, H. Y., & Rui, X. X. (2020). Gradation affects basic mechanical characteristics of Chinese calcareous sand as airport subgrade of reefs. *Marine Geore-*

sources Geotechnology, 38(6), 706–715. https://doi.org/10.1080/1064119x.2019.1614122.

Shen, X., Shen, Y., Xu, J. H., & Liu, H. L. (2022). Influence of the fractal distribution of particle size on the critical state characteristics of calcareous sand. *Fractal and Fractional, 6*(3), 165.

Song, Y. Q., Ma, H. F., Yang, J. K., Zheng, J. J., Yang, J. T., & Bao, W. (2022). Dynamic mechanical behaviors and failure mechanism of lignite under SHPB compression test. *Sustainability, 14*(17), 10528.

Tan, T. J., Wang, E. Y., Wang, X. R., & Yao, W. L. (2023). Study on the electrical impedance response and conductivity mechanism of coal mass rupture under impact load. *Measurement, 219*, 113164. https://doi.org/10.1016/j.measurement.2023.113164.

Tian, H., Li, Z. H., Yin, S., Lei, Y. Y., Niu, Y., Wang, X. Y., Zang, Z. S., & Gu, Z. J. (2023). Research on infrared radiation response and energy dissipation characteristics of sandstone crushing under impact load. *Engineering Geology, 322*, 107171.

Wang, H. C., Zhao, J., Li, J., et al. (2021a). Dynamic mechanical properties and fracturing behaviour of concrete under biaxial compression. *Construction and Building Materials, 301*, 124085.

Wang, H. C., Zhao, J., Li, J., Wang, H. J., Braithwaite, C. H., & Zhang, Q. B. (2022b). Fracturing and AE characteristics of matrix-inclusion rock types under dynamic Brazilian testing. *International Journal of Rock Mechanics and Mining Sciences, 157*, 105164.

Wang, J., Ma, L., Zhao, F., Lv, B. G., Gong, W. L., He, M. C., & Liu, P. (2022a). Dynamic strain field for granite specimen under SHPB impact tests based on stress wave propagation. *Underground Space, 7*(5), 767–785.

Wang, T., Song, Z. P., Yang, J. Y., Zhang, Q., & Cheng, Y. (2021d). A study of the dynamic characteristics of red sandstone residual soils based on SHPB tests. *Ksce Journal of Civil Engineering, 25*(5), 1705–1717.

Wang, X. R., Asem, P., Hu, C., & Labuz, J. F. (2021b). Microcracking in tensile fracture of a brittle rock. *Engineering Fracture Mechanics, 251*, 107789.

Wang, X. R., Wang, E. Y., Liu, X. F., & Zhou, X. (2021c). Failure mechanism of fractured rock and associated acoustic behaviors under different loading rates. *Engineering Fracture Mechanics, 247*, 107674.

Wang, X. F., Hu, S. B., Wang, E. Y., Zhang, Q., & Liu, B. (2023). Experimental research and energy analysis of a new type of dry ice powder pneumatic rock breaking technology. *International Journal of Mining Science and Technology, 33*(4), 423–435. https://doi.org/10.1016/j.ijmst.2022.12.010.

Wei, J., Liao, H. L., Li, N., Liang, H. J., Chen, K. F., Yan, H., Fan, Y. G., & Zhao, X. H. (2023). Effect of the three-dimensional static pre-stress on the dynamic behaviours of conglomerate: True triaxial Hopkinson pressure bar tests. *Geoenergy Science and Engineering, 227*, 211810.

Weng, L., Wu, Z. J., Liu, Q. S., & Wang, Z. Y. (2019). Energy dissipation and dynamic fragmentation of dry and water-saturated siltstones under sub-zero temperatures. *Engineering Fracture Mechanics, 220*, 106659.

Wu, X. G., Wang, S. R., Yang, J. H., Zhao, J. Q., & Chang, X. (2022). Damage characteristics and constitutive model of lightweight shale ceramsite concrete under static-dynamic loading. *Engineering Fracture Mechanics, 259*, 108137.

Xie, H. P., & Gao, F. (2000). The mechanics of cracks and a statistical strength theory for rocks. *International Journal of Rock Mechanics and Mining Sciences, 37*(3), 477–488.

Xie, H. P., Li, C., He, Z. Q., Li, C. B., Lu, Y. Q., Zhang, R., & Gao, F. (2021). Experimental study on rock mechanical behavior retaining the in situ geological conditions at different depths. *International Journal of Rock Mechanics and Mining Sciences, 138*, 104548.

Xie, H., & Zhou, H. W. (2008). Application of fractal theory to top-coal caving. *Chaos Solitons & Fractals, 36*(4), 797–807.

Xu, S. L., Shan, J. F., Zhang, L., Zhou, L. J., Gao, G. F., Hu, S. S., & Wang, P. F. (2020). Dynamic compression behaviors of concrete under true triaxial confinement: An experimental technique. *Mechanics of Materials, 140*, 103220.

Yang, H. Z., Wang, E. Y., Cheng, D. Q., Wang, X. R., Li, B. L., Song, Y., Wang, DM., & Liu, W. Z. (2023). Characteristics of energy evolution and acoustic emission response of concrete under the action of acidic drying-saturation processes cycle. *Journal of Building Engineering, 74*, 106928. https://doi.org/10.1016/j.jobe.2023.106928.

Yin, Z. Q., Li, X. B., Jin, J. F., He, X. Q., & Du, K. (2012). Failure characteristics of high stress rock induced by impact disturbance under confining pressure unloading. *Transactions of Nonferrous Metals Society of China, 22*(1), 175–184.

You, W., Dai, F., & Liu, Y. (2022a). Experimental and numerical investigation on the mechanical responses and cracking mechanism of 3D confined single-flawed rocks under dynamic loading. *Journal of Rock Mechanics and Geotechnical Engineering, 14*(2), 477–493. https://doi.org/10.1016/j.jrmge.2021.09.006.

You, W., Dai, F., Liu, Y., & Yan, Z. L. (2022b). Effect of confining pressure and strain rate on mechanical behaviors and failure characteristics of sandstone containing a pre-existing flaw. *Rock Mechanics and Rock Engineering, 55*(4), 2091–2109.

Yu, X., Chen, L., Fang, Q., Zhang, J. H., Guo, D., & Hou, X. F. (2019). Determination of attenuation effects of coral sand on the propagation of impact-induced stress wave. *International Journal of Impact Engineering, 125*, 63–82.

Zang, Z. S., Li, Z. H., Niu, Y., Tian, H., Zhang, X., Li, X. L., & Ali, M. (2021). Energy dissipation and electromagnetic radiation response of sandstone samples with a pre-existing crack of various inclinations under an impact load. *Minerals, 11*(12), 1363.

Zang, Z., Li, Z., Zhao, E., Kong, X., Niu, Y., & Yin, S. (2023). Electric potential response characteristics and constitutive model of coal under axial static load–dynamic load coupling. *Natural Resources Research*. https://doi.org/10.1007/s11053-023-10261-w.

Zhang, Q. B., & Zhao, J. (2014). A review of dynamic experimental techniques and mechanical behaviour of rock materials. *Rock Mechanics and Rock Engineering, 47*(4), 1411–1478.

Zhang, X., Li, Z. H., Wang, X. R., Wang, H., Li, B. L., & Niu, Y. (2022). Thermal effect on the fracture behavior of granite using acoustic emission and digital image correlation: An experimental investigation. *Theoretical and Applied Fracture Mechanics, 121*, 103540.

Zhao, Y. X., Gong, S., Hao, X. J., Peng, Y., & Jiang, Y. D. (2017). Effects of loading rate and bedding on the dynamic fracture toughness of coal: Laboratory experiments. *Engineering Fracture Mechanics, 178*, 375–391.

Zhou, T., Han, Z. Y., Li, D. Y., & Chen, J. R. (2022). Experimental study of the mechanical and fracture behavior of flawed sandstone subjected to coupled static-repetitive impact loading. *Theoretical and Applied Fracture Mechanics, 117*, 103161.

Zhou, X., Liu, X. F., Wang, X. R., Liu, Y. B., Xie, H., & Du, P. F. (2023). Acoustic emission characteristics of coal failure under triaxial loading and unloading disturbance. *Rock Mechanics and Rock Engineering, 56*(2), 1043–1061.

Zhu, Q., Li, D., & Wang, W. J. (2021). Mechanical behavior and permeability evolution of sandstone with confining pressure after dynamic loading. *Geomechanics and Geophysics for Geo-Energy and Geo-Resources, 7*(3), 1–20.

Zhu, Q. Q., Li, X. B., Li, D. Y., & Ma, C. D. (2022). Experimental investigations of static mechanical properties and failure characteristics of damaged diorite after dynamic triaxial compression. *International Journal of Rock Mechanics and Mining Sciences, 153*, 105106.